

A study on observing, detecting, and determining objects in low earth orbit using optical telescope system

Huy Le Xuan¹, Su Nguyen Tien¹, Quan Trinh Hoang¹, Soat Le The¹, Khang Trinh Van¹, Tu Tran Anh^{1,2}, Linh La Thuy^{1,2}

¹Vietnam National Space Center, Vietnam Academy of Science and Technology, Hanoi, Vietnam

²University of Science and Technology of Hanoi, Vietnam Academy of Science and Technology, Hanoi, Vietnam

Article Info

Article history:

Received Dec 25, 2023

Revised May 14, 2024

Accepted Jun 1, 2024

Keywords:

Artificial intelligence

Low earth orbit

Optical telescope

Simulation

Space object

Space surveillance and tracking

ABSTRACT

Problems of space debris, space security threats and space accidents are an escalating topic that is drawing attention from scientists and researchers worldwide. Based on the practical demand for detecting and surveilling objects in Earth's orbit in the Vietnam's sky area, the research group has designed a space monitoring system to detect and identify orbiting objects using optical telescopes. The idea of this system is to utilize wide and narrow field-of-view (FOV) optical telescope systems to observe and identify the trajectory of orbiting objects. After an image of an unknown object is captured with a wide FOV telescope, an analyzing algorithm will process and predict the trajectory of it, with support of artificial intelligence, and determine whether there is the appearance of an uncataloged object. If it is affirmative, the narrow telescope system will adapt to a new attitude to track the object from predicted trajectory and gather information for future use. Constructing and validating of this monitoring system deployed by the research group are described in this paper.

This is an open access article under the [CC BY-SA](#) license.



Corresponding Author:

Huy Le Xuan

Vietnam National Space Center, Vietnam Academy of Science and Technology

Hanoi, Vietnam

Email: lxhuy@vnsc.org.vn

1. INTRODUCTION

The exploration and utilization of low earth orbit (LEO) have become the integral components of contemporary space industry, with applications ranging from defense, earth observation, communication to scientific research [1]. The annual space environment report by the European Space Agency (ESA) shows that by the end of 2022, this orbital region was filled with nearly 20,000 objects, from functioning satellites to space debris [2]. Therefore, the effective monitoring of these objects via space surveillance and tracking (SST) system has become essential for avoiding incidents and ensuring the sustainable use of space resources. The main techniques employed in present SST systems are radar and optical, with radar being the dominant one since it is independent with time and weather conditions [3]. Nevertheless, the use of optical telescopes to observe, detect and identify LEO objects has gained an increasing interest in recent years, thanks to the low cost, simple installment and advancement in data processing tools [4]. The DEIMOS group constructed the DEIMOS sky survey observatory to track objects using optical telescopes [5]. The Korea Astronomy and Space Science Institute (KASI) developed a global network called OWL-Net with 0.5 m wide-field telescopes placed across five countries to track satellites in different global regions [6]. Kamiński *et al.* [7] used two telescopes located in Poland and the US for the same goal.

Considering all the studies of the previous work, with the demanding command of SST and the available facility, the Vietnam National Space Center (VNSC) selected optical telescopes as the foundation to construct an optimized SST system for Vietnam to monitor Vietnam's airspace and predicting the possible threats for Vietnam's future satellites. In this paper, we describe our newly built SST system with all the vital features: taking and processing images, detecting new objects, and predicting the objects' orbit. These SST system's features on small-scale SST can also be seen in previous works by [8]–[11], but without a threshold for the decision of a new object. The decision of whether one is a new object or not is the key problem of the system. Firstly, the rising number of newly launched satellites requires the database of known objects to be updated daily, so that the defined objects will not be misunderstood as undefined ones. This database is a set of calculated and recorded satellite's two-line element (TLE) [12]. TLE contains information about both the shape of the orbit and the position of the satellite in the orbit, with the main characteristics such as inclination, eccentricity, right ascension of ascending node (RAAN), argument of perigee and the extrapolation of the satellite's position at any time after the TLE's epoch time is possible using the propagation model such as SPG4 or SPG8. This format makes the procedure of monitoring and tracking convenient with known objects as will be used throughout our work. Secondly, an object itself will not maintain its orbit but fluctuate around since it suffers from perturbation from the Earth's atmosphere and other objects in its orbit. This leads to another major problem of an SST is that the imaging of the satellite will always suffer from certain errors. Therefore, a thorough reconstruction of the orbital elements and also long-term observation is required. In the field, the orbital parameters are usually using either commercial software such as NASA GEODYN [13], Ansys ODTK [14], or self-developed programs. The application of machine learning in SST data processing and management has been considered [15]–[17], but is still limited.

Considering the challenges, our objective is to integrate the SST system as a whole, obtain images using both wide and narrow-field telescopes, and then use the Gauss algorithm [18] to generate TLE sets for long-time tracking with our self-developed Python program. Parallely, we extract characteristics of the orbit from the Hough algorithm [19] and train the support vector machine (SVM) [20], thus improving the decision of the system on the novelty of an orbiting object. The workflow of the system and the feasibility of the system will also be discussed. The remaining parts of the paper is structured as follows: section 2 gives the overview and working procedure of the system, as well as the theory and integration of SVM. The results are presented in section 3 and the paper ends with concluding remarks in section 4.

2. SYSTEMS OVERVIEW AND METHODS

2.1. System overview

We utilize the available resources of telescopes and computing systems to build a system that allows continuous tracking and data transferring. There are three main parts of the system: wide-field telescopes, narrow-field telescopes, and computing and control systems. They are constructed following the schematic in Figure 1, with the main components listed in Table 1.

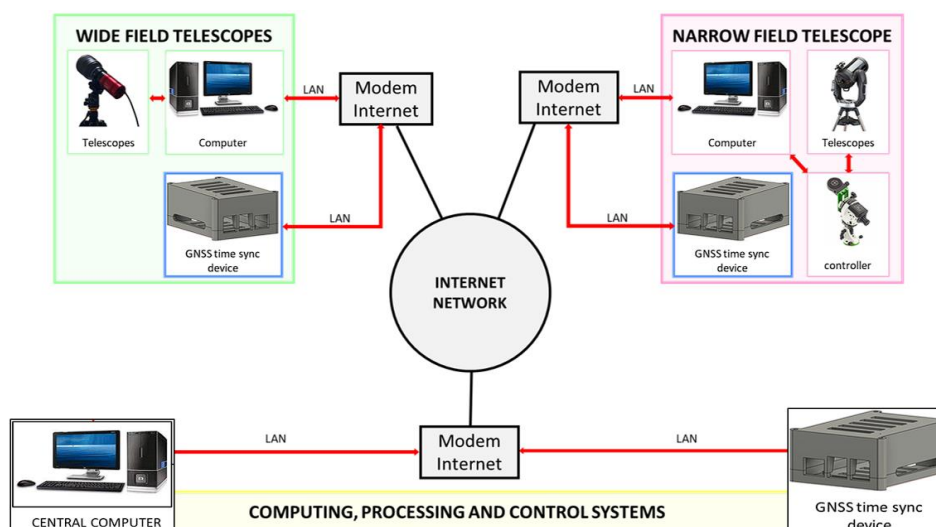


Figure 1. Diagram of the telescope system

Table 1. Subsystems and components of the telescope system

No	Sections	Components	Functions
1	Observation telescope system	- Wide-field telescope - Control computer - Time synchronization device	Sky monitoring photography function, providing image data to the central computer
2	Surveillance telescope system	- Narrow-field telescopes - Control computer - Time synchronization device - System controller	Receive control commands from the central computer, perform the function of taking pictures of the sky at the time and location where objects are likely to appear calculated by the central computer
3	Computing, processing and control system	- High performance computer - Time synchronization device	Manage and process information about the object's trajectory, perform calculations and simulations and issue warnings and notifications to users

The PlaneWave CDK24 astronomical telescope with a $3.2^\circ \times 2.13^\circ$ FOV [21] is utilized as a wide-field telescope for observation system, while the 0.5 m RC500 telescopes with $0.53^\circ \times 0.53^\circ$ FOV [22], equipped with FLI-PL 16803 camera are used as narrow-field telescope for surveillance system. A high-performance computer processes all the data using self-developed software and machine learning algorithms. All components are time synchronized using GNSS network time servers developed in Anh *et al.* [23] to provide accurate timing and high-security time synchronization.

The working procedure of the whole system is depicted in Figure 2. First, the wide FOV telescope, positioned at observation station 1, captures images of a predetermined area in the sky. The images are then analyzed by image processing software, which detects passing objects based on the bright streaks. If bright streaks appear in the images, the software extracts the capture time, exposure time, right ascension (Ra), and declination (Dec) parameters from the images. With this information, the software generates simulated orbital images of all active satellites that may be visible in the FOV of the telescope, then compares them with the captured image using a machine learning approach to identify the objects. If the objects are unknown from the current database, the image data is then processed by satellite orbit prediction software. This software enables the determination of the object's flight trajectory and records its appearance history. In case the objects move toward observation station 2 with a narrow FOV telescope, the computer controlling the telescope adjusts the Azimuth (Az) and Elevation (El) angles and specifies the capture time to capture the object. The new images are then put back into the image processing software, in which the discrepancies between calculated information and the captured images are analyzed to evaluate detailed information about the object.

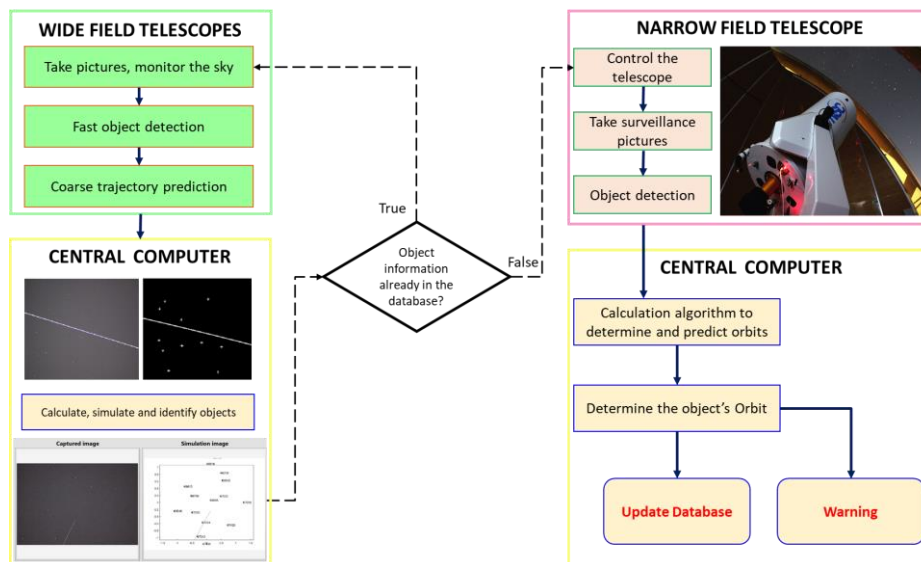


Figure 2. Process of observing, detecting and determining object orbits

2.2. Solution to control telescope system to track the object's orbit

When an unidentified object is detected at time t_1 , a linear calculation will be made in the satellite trails direction, so that the narrow-field telescope can follow the satellite and catch it the next times at t_2 and

t_3 . With the information from the three captures of the object, we use Gauss method following the geometry in Figure 3 and print out its TLE. This TLE will be used as the first estimation of the object and will be used to capture the object in the future. This process enables the system to continuously monitor objects with precision using regularly updated data.

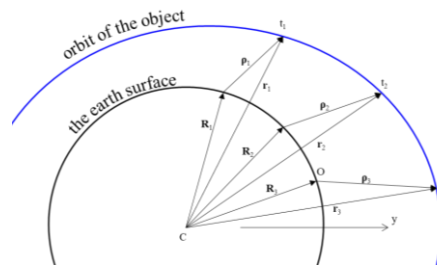


Figure 3. Position of the satellite at the time of image capturing

2.3. Image simulation

Knowing the location, attitude, and FOV of a telescope at a certain time, we can simulate the image that the telescope may capture. In case the captured image has unclear information (unknown Az/El), a supplementary astrometry step is used so that the real image's center (Ra/Dec) can still be calculated and converted to the local frame of the observatory. This simulation of the sky will contain the stars from the Hipparcos catalog [24], with the visible streak of known satellites propagated using SPG4 [25]. By comparing the simulated image and the real image, visually, we can detect if any new object flies over the FOV. The accuracy of the simulated images has been verified with real images, as illustrated in Figures 4(a) and (b).

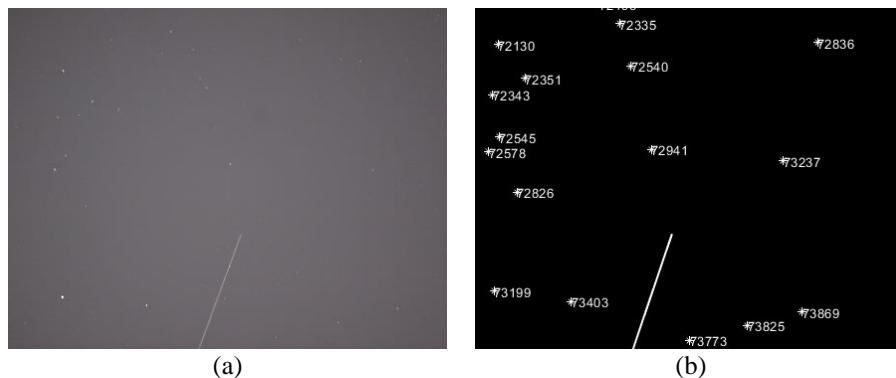


Figure 4. Images of H-2AR_B-38341 viewed at (109.21E, 13.72N) on 12 May 2022 at 12:21:49.549 UTC; (a) real image taken by Quy Nhon Telescope and (b) simulated image

2.4. Characteristics extraction of satellite trails

The captured images need to undergo image preprocessing steps such as noise filtering, contrast enhancement, resizing to match the simulated image, conversion to grayscale, and then binary image conversion. Afterward, the Canny algorithm [26] is used to detect the edges of the objects. The idea behind this algorithm is based on the change in the gradient to identify edges, as there is a variation in pixel values when passing through edges. Finally, the Hough algorithm [27] is employed to determine the straight lines, as in Figure 5(a). The Hough algorithm provides us with information about the straight line, such as the pixel values at the beginning and end of the line, the angle θ formed with the horizontal axis, and the distance from the origin ρ . Leveraging these parameters, we define the features of the data in Figure 5(b).

The next step is to determine the difference between the simulated and captured images, based on the the two trails. To make the comparison, the research group employs the SVM algorithm. The idea of the method is illustrated in Figure 6(a). If the two trails in the simulated and captured images have similar

characteristics, they are classified as the identified trail (class 1). If these features differ significantly, they are assigned to the unidentified trail (class 2). The dividing hyperplane $y = w \times x + b$ between these two classes could be found by maximizing the total distance of points to the line. The database is the crucial first step in addressing machine learning problems. Figure 6(b) illustrates the main steps in executing the solution to a machine learning problem.

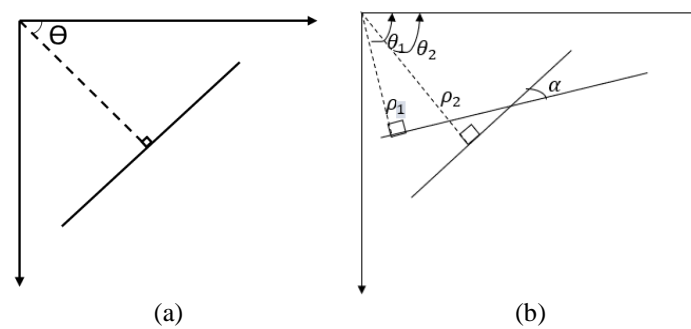


Figure 5. Illustration of Hough algorithm: (a) extracts the angle and distance of a satellite trail then (b) extracts the features of two trails for comparison

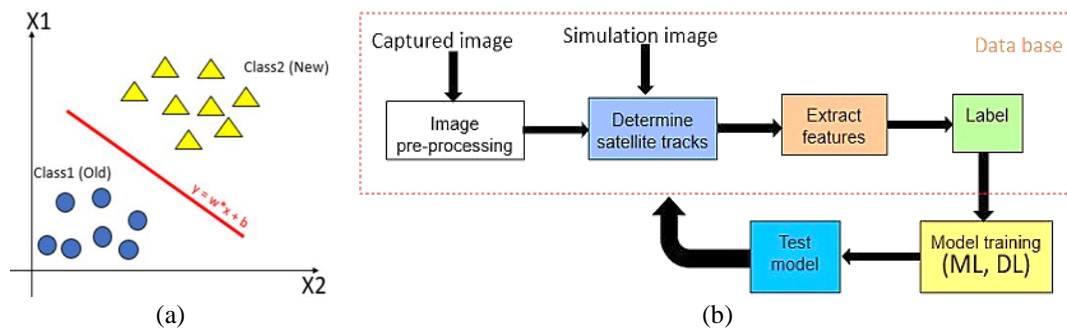


Figure 6. SVM implementation: (a) classification of images into two classes and (b) machine learning solution workflow

3. RESULTS AND DISCUSSION

3.1. Accuracy of Gauss method for orbit prediction

Figure 7 indicates the procedure for generating the sample TLEs for simulation as well as for training the SVM model. We start with a reference TLE from Celestrak's brightest satellites representing a known and observable satellite (<https://www.celestrak.com>). The epoch time of the TLEs must be within 3 days of the time of the 'virtual' capture so that the real satellite trails will not have too much deviation. The coordinates of the satellite at any time could be extracted by propagating using SPG4. Besides, with the known information about the telescope that is used for observation (its location, attitude, and FOV), we could simulate the sky image that could be captured at any moment, including the stars and the satellite trails. Hence we then choose three epoch times, named t_1 , t_2 , and t_3 , as portrayed in Figure 3, spaced 40 seconds apart. At these epoch times, the satellite is visible to the telescope, and the corresponding Az/EI angles of the telescope will be calculated. Subsequently, these modified sets are input into the Gauss algorithm, as previously described, to generate a TLE test.

The Gauss algorithm has been tested via this procedure, using 100 satellites, under the condition that no noise is added to the system. The result shows that in comparison with the original TLE element-wise subtraction, the inclination has very small deviation $\mu = 0.005$, $\sigma = 0.0359$ (in degrees), the errors in eccentricity ($\mu = 6e - 4$, $\sigma = 0.0013^\circ$) and semimajor axis ($\mu = -9.1 \text{ km}$, $\sigma = 13.13 \text{ km}$) are also insignificant, and can be concluded that orbit shape can be defined well with high accuracy. On the other hand, to account for potential noise arising from imperfections in the observing system or variations in the satellite's orbit, Gaussian noise (0, 1/30) and $N(0, 1/300)$ is added to the Az/EI sets as shown in Figure 7. The test TLEs (1,000 test TLE for each TLE_{true}) are generated and added the mentioned noise, and then compared

to the TLE_{true} by two methods: i) by element-wise subtraction and ii) by Hough algorithm. From Table 2, we observe that not all elements exhibit Gaussian shifts, with unpredictability particularly evident in the argument of perigee and mean motion because in nearly circular, the perigee of the orbit is ill-defined, therefore these values are vague to a predictor. This method is robust, but it is very sensitive to the accuracy of the calculation since all the elements are linked together. We can see that the errors of the system can bring up wrong values to the generated TLE.

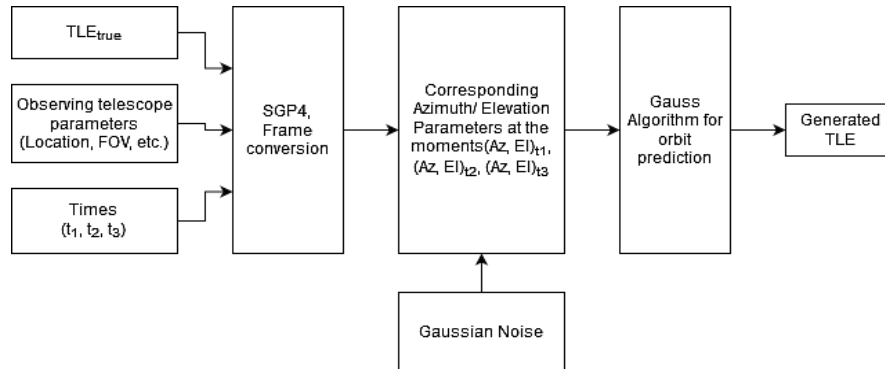


Figure 7. Procedure of generate test TLE

Table 2. Residuals of three satellite data sets: PCSAT, COSMOS-482, and NOAA-19

			i (deg)	Ω (deg)	e (deg)	ω (deg)	M (deg)	SA (km)
PCSAT	0.1	Mean	0.031	-0.383	0.230	-44.337	-0.696	3105
		1-sigma	0.332	0.342	0.190	13.219	5.931	20 958
	0.01	Mean	0.032	-0.406	0.022	-43.681	-0.026	16
		1-sigma	0.035	0.035	0.017	11.676	0.629	212
COSMOS-482	0.1	Mean	-0.768	-2.244	0.393	-27.618	7.525	5918
		1-sigma	1.026	0.538	0.240	13.109	10.249	76271
	0.01	Mean	0.024	-1.827	0.053	-9.962	0.205	101
		1-sigma	0.162	0.067	0.068	20.761	2.698	1170
NOAA-19	0.1	Mean	-0.036	0.470	0.126	-47.313	-0.127	390
		1-sigma	0.266	0.697	0.103	21.789	3.498	1821
	0.01	Mean	-0.009	0.440	0.012	-42.069	0.074	-22
		1-sigma	0.027	0.071	0.009	28.238	0.358	121

3.2. Support vector machine and orbit detection

Alternatively, to overcome the problem with the previous method, simulation with images offers a clearer visualization of orbital trajectories and can withstand larger amounts of noise compared to previous methods, effectively bypassing the challenge of undefined orbital perigees. Nonetheless, this approach demands significantly more simulation and computational resources. These characteristics of the trail, which are angles and distances derived from the images, are treated as training data for the SVM framework. Sets of test TLEs from section 3.2 will be considered as trails of the same object, i.e. will be detected as “old” object. Subsequently, the SVM analyzes these features to make informed determinations regarding the novelty of the observed objects if any strange trails appear in the image. The decision boundary of the SVM is computed using MATLAB. In general, the result of the SVM considers the trails which have angles difference smaller than 5° and distance difference smaller than 30 pixels as the old object, given the image size reduced to 434×343 pixels.

At 19:10:30 on May 12, 2022, at Quy Nhon Observatory (13.718, 109.213), using the wide FOV telescope PlaneWave CDK24, the group took the images with an exposure time of 4 seconds and detected a satellite streak. The streak was caused by the satellite CZ-4BR_B-27432, with the following TLE data: i) 1 27432U 02024C 22130.83991647 .00000022 00000+0 35169-4 0 9992 and ii) 2 27432 99.0646 155.4106 0050777 24.1126 148.5409 14.14136574 31504. Later, at 19:21:30 on May 12, 2022, at the same location, we detected another satellite streak in the image. This streak is determined to be of the satellite H-2AR_B-38341, with the following TLE data: i) 1 38341U 12025E 22130.59854921 .00000875 00000+0 10824-3 0 9997; and ii) 2 38341 98.5098 343.3468 0055126 167.2367 193.0256 14.84626597540032. Figures 8(a) and (b) show the simulated images, captured images and classification results from two detections the angle θ are 3° and 5° , and distance ρ are 2.59 and 22.76, respectively. With the trained data in

the SVM, these values are regarded as belonging to the "old" object. The model is considered robust to be implemented in more advanced tasks.

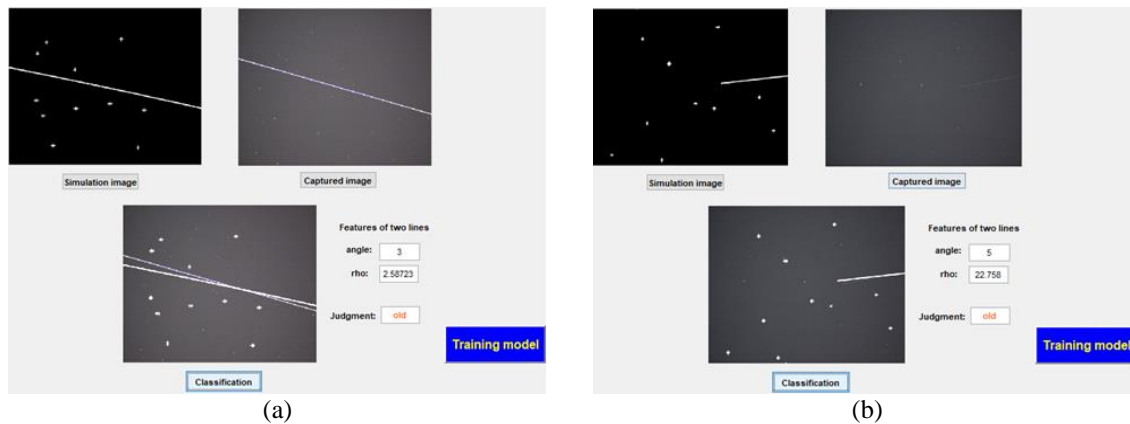


Figure 8. Captured image, simulated image, and classification from; (a) first detection and (b) second detection

3.3. Trajectory prediction

In this section, we evaluate the trajectory prediction algorithm to see whether it could track unknown detected object. The test data are the TLE data of 10 satellites from NOAA-12 to NOAA-21. For each satellite, we assign a random observation location, then setup the telescope tracking by determining azimuth and elevation angles of the telescope at two closely instances T0–5 second and T0, as in Table 3. The Az and El angles of the telescope at T0+20s and T0+40s will be predicted by the model, and they are validated using Orbitron software [28]. The results of predicting the position of the telescope to observe the satellite after 20 seconds are presented in Table 4 and after 40 seconds in Table 5, respectively.

Table 3. Setup data

Case	Satellite	Location Latitude	Point 1 (T0-5s)		Point 2 (T0)		Location Elevation	Point 1 (T0-5s)		Point 2 (T0)	
			Longitude	Azimuth	Azimuth	Elevation		Azimuth	Elevation	Azimuth	Elevation
1	NOAA-12	19	-115.178	323.1	17.6	322.1	18				
2	NOAA-13	6	24.622	283.8	21.5	284.9	21.2				
3	NOAA-14	9.5	31.222	69.8	26.4	68.4	26.3				
4	NOAA-15	-42.5	88.822	325.4	22.8	325.8	22.1				
5	NOAA-16	37.5	-88.778	32.6	22.5	33.1	23.1				
6	NOAA-17	-24	-6.578	48.6	27.5	47.2	27				
7	NOAA-18	-23	123.022	75.5	26.7	74	26.7				
8	NOAA-19	19.5	105.222	327.4	33.4	328.1	32.4				
9	NOAA-20	12	-10.178	108.6	27.9	107.2	28.4				
10	NOAA-21	-5	168.022	345.5	20.5	344.9	21.1				

Table 4. Orientation of the telescope after 20s

Case	Point 3 (T0+20s)					
	Azimuth		Absolute error (deg)	Elevation		Absolute error (deg)
	Our model	Orbitron		Our model	Orbitron	
1	318.1	317.9	0.2	19.6	19.3	0.3
2	289.3	289.3	0	20	20	0
3	62.8	62.5	0.3	25.9	25.7	0.2
4	327.4	327.1	0.3	19.3	19.5	0.2
5	35.1	35.6	0.5	25.5	25.9	0.4
6	41.6	42.2	0.6	25	25.1	0.1
7	68	68.2	0.2	26.7	26.1	0.6
8	331	330.4	0.6	28.4	28.7	0.3
9	101.6	101.3	0.3	30.4	30.2	0.2
10	342.5	342.2	0.3	23.5	23.6	0.1
Mean			0.33	Mean		0.24
Standard deviation			0.19	Standard deviation		0.17
Worst case			0.6	Worst case		0.6

Table 5. Orientation of the telescope after 40s

Case	Azimuth			Point 4 (T0+40s)		
	Our model	Orbitron	Absolute error (deg)	Our model	Orbitron	Absolute error (deg)
1	314.1	313.3	0.8	21.2	20.6	0.6
2	293.7	293.4	0.3	18.8	18.6	0.2
3	57.2	56.9	0.3	25.5	24.9	0.6
4	329	328.3	0.7	16.5	17.1	0.6
5	37.1	38.5	1.4	27.9	28.9	1
6	36	37.7	1.7	23	23	0
7	62	62.5	0.5	26.7	25.2	1.5
8	333.7	332.2	1.5	24.4	25.5	1.1
9	96	94.7	1.3	32.4	31.7	0.7
10	340.1	339.1	1	25.9	26.3	0.4
Mean			0.95	Mean		0.67
Standard deviation			0.51	Standard deviation		0.44
Worst case			1.7	Worst case		1.5

From Table 3, when predicting the telescope position after 20 seconds, the mean error of Az and El angles are 0.33 and 0.24, with standard deviation of 0.19 and 0.17, respectively, the maximum error for both angles is 0.6. It should be noted that only absolute error in degree is important for this application, since if the deviation is larger than the telescope FOV, the telescope may miss the object. After 40 seconds, as shown in Table 4, the errors are higher in all criteria, with the maximum value is 1.7° in Az, and 1.5° in El. From these results, for a telescope with FOV of 2° , it is feasible to track and capture images of the object during 40 seconds after it enters the region. This simulation result helps in sizing the telescope and designing the observation mission.

4. CONCLUSION

We have successfully demonstrated the capability of the telescope system in capturing sky images with orbiting objects, and developed a machine learning model to process the images, as well as predicting satellite orbit. With the images obtained of an orbiting object, its TLE can be generated with high accuracy. The integration of SVM model has supported the decision-making process and helped the automatism of the SST system. In the future, more real data, i.e., images taken by the telescopes, will provide more data to train the system with higher accuracy.

ACKNOWLEDGEMENTS

This work is supported by Vietnam National Space Center through the Vietnam Academy of Science Technology project titled "Research on Method of Observation, Detection, and Identification of Objects in Orbit around Earth Using Optical Telescope - ĐL0000.01/21-22" and Vietnam Academy of Science and Technology (VAST) under grant No.NCVCC39.01/22-23.




REFERENCES

- [1] W. Ley, K. Wittmann, and W. Hallmann, *Handbook of space technology*. Chichester, UK: Wiley, 2009.
- [2] European Space Agency, "ESA's annual space environment report," 2024.
- [3] H. Klinkrad, *Space debris: models and risk analysis*, vol. 53, no. 9. Springer Berlin, Heidelberg, 2006, doi: 10.1007/3-540-37674-7.
- [4] B. Lal, A. Balakrishnan, B. M. Caldwell, R. S. Buenconsejo, and S. A. Carioscia, *Global trends in space situational awareness (SSA) and space traffic management (STM)*, vol. 10. Institute for Defense Analyses, 2018.
- [5] N. Sanchez-Ortiz, J. N. Torres, R. Dominguez-Gonzalez, and G. N. Lopez, "Accurate optical observation of space objects in IEO regime," *The Advanced Maui Optical and Space Surveillance Technologies Conference*, Wailea, Maui, Hawaii, September 11-14, 2018.
- [6] J.-H. Park *et al.*, "OWL-Net: a global network of robotic telescopes for satellite observation," *Advances in Space Research*, vol. 62, no. 1, pp. 152–163, Jul. 2018, doi: 10.1016/j.asr.2018.04.008.
- [7] K. Kamiński *et al.*, "Low LEO optical tracking observations with small telescopes," in *1st NEO and Debris Detection Conference*, vol. 1, no. 1, 2019.
- [8] T. Hasenohr, "Initial detection and tracking of objects in low earth orbit," M.S. thesis, German Aerospace Center Stuttgart, Institute of Technical Physics, Stuttgart, Germany, 2016.
- [9] T. P. G. Wijnen, R. Stuik, M. Rodenhuis, M. Langbroek, and P. Wijnja, "Using all-sky optical observations for automated orbit determination and prediction for satellites in low earth orbit," *arXiv*, 2020, doi: 10.48550/arXiv.2004.08137.
- [10] J. Utmann, M. G. D. Vesselinova, and O. R. Fernandez, "Airbus robotic telescope," in *1st NEO and Debris Detection Conference*, 2019, pp. 22–24.
- [11] R. G. Danescu, R. Itu, M. P. Muresan, A. Rednic, and V. Turcu, "SST anywhere—a portable solution for wide field low earth orbit surveillance," *Remote Sensing*, vol. 14, no. 8, 2022, doi: 10.3390/rs14081905.




- [12] D. A. Vallado and P. J. Cefola, "Two-line element sets—practice and use," in *63rd International Astronautical Congress*, 2012, pp. 1–14.
- [13] B. Putney, R. Kolenkiewicz, D. Smith, P. Dunn, and M. H. Torrence, "Precision orbit determination at the NASA Goddard Space Flight Center," *Advances in Space Research*, vol. 10, no. 3–4, pp. 197–203, 1990, doi: 10.1016/0273-1177(90)90350-9.
- [14] D. A. Vallado, R. S. Hujsak, T. M. Johnson, J. H. Seago, and J. W. Woodburn, "Orbit determination using ODTK version 6," in *4th International Conference on Astrodynamics Tools and Techniques*, 2010, pp. 3–6.
- [15] A. Montanaro, T. Ebisuzaki, and M. Bertaina, "Stack-CNN algorithm: a new approach for the detection of space objects," *Journal of Space Safety Engineering*, vol. 9, no. 1, pp. 72–82, 2022, doi: 10.1016/j.jsse.2022.01.001.
- [16] M. Caceres, J. Salazar, M. Sacchi, D. Rijlaarsdam, L. Buckley, and F. Buckley, "Hybrid edge-cloud ai accelerated astrometric reduction pipeline for agile near-real time in-situ SST," *Nebula Public Library*, pp. 1–11, 2022.
- [17] C. Manfletti, M. Guimarães, and C. Soares, "AI for space traffic management," *Journal of Space Safety Engineering*, vol. 10, no. 4, pp. 495–504, 2023, doi: 10.1016/j.jsse.2023.08.007.
- [18] H. D. Curtis, "Preliminary orbit determination," in *Orbital Mechanics for Engineering Students*, Elsevier, 2010, pp. 255–317.
- [19] S. Ding, H. Wang, D. Chen, T. Fu, and M. Gao, "An improved method for dim space debris detection based on hough transform," *International Conference on Signal Processing Proceedings, ICSP*, pp. 1534–1538, 2016, doi: 10.1109/ICSP.2016.7878083.
- [20] C. Cortes and V. Vapnik, "Support-vector networks," *Machine Learning*, vol. 20, no. 3, pp. 273–297, Sep. 1995, doi: 10.1007/BF00994018.
- [21] PlaneWave Instruments, "CDK24 Brochure." 2019.
- [22] N. T. Thao, N. T. Dung, P. V. Loc, N. T. K. Ha, and P. N. Diep, "The 50 cm telescope of Hoa Lac observatory: an introduction," *Vietnam Journal of Science, Technology and Engineering*, vol. 61, no. 4, pp. 14–28, 2019, doi: 10.31276/vjste.61(4).14-28.
- [23] T. T. Anh, T. N. Van, and H. Le Xuan, "Developing a network time server for LEO optical tracking," *Bulletin of Electrical Engineering and Informatics (BEEI)*, vol. 11, no. 3, pp. 1308–1316, 2022, doi: 10.11591/eei.v11i3.3636.
- [24] M. A. C. Perryman *et al.*, "The hipparcos catalogue," *Astronomy and Astrophysics*, vol. 323, no. 1, pp. 49–52, 1997.
- [25] D. Vallado and P. Crawford, "GP4 orbit determination," *AIAA/AAS Astrodynamics Specialist Conference and Exhibit*, 2008.
- [26] J. Canny, "A computational approach to edge detection," *IEEE Transactions on Pattern Analysis and Machine Intelligence*, no. 6, pp. 679–698, Nov. 1986, doi: 10.1109/TPAMI.1986.4767851.
- [27] R. O. Duda and P. E. Hart, "Use of the Hough transformation to detect lines and curves in pictures," *Communications of the ACM*, vol. 15, no. 1, pp. 11–15, Jan. 1972, doi: 10.1145/361237.361242.
- [28] S. Stoff, "Orbitron - satellite tracking system." 2007, [Online]. Available: <http://www.stoff.pl/>. (Accessed: Dec. 12, 2023).

BIOGRAPHIES OF AUTHORS






Huy Le Xuan    received Ph.D. degree in mechanical and aerospace engineering from Tokyo Institute of Technology in 2014. He has been working at VNSC since 2011 at Department of Space Systems Design. Currently, he is the Vice Director General of VNSC. His research interests are development of small satellites for earth observation, system engineering, satellite attitude determination and control, optimal estimation of dynamics systems. Involved projects: PicoDragon (1 kg satellite of VNSC), MicroDragon (50 kg satellite of VNSC), and NanoDragon (4 kg satellite of VNSC). He can be contacted at email: lxhuy@vnsc.org.vn.






Su Nguyen Tien    received M.Eng. degree in space engineering from Kyushu Institute of Technology in 2016. Since 2014, he has been working at Vietnam National Space Center as researcher. His research interests are electrical power supply system (EPS), 3D printing, and LabVIEW software development. He can be contacted at email: ntsu@vnsc.org.vn.






Quan Trinh Hoang    received M.Eng. degree in aerospace engineering from Tohoku University in 2015. Since 2011, he has been working at Vietnam National Space Center as a researcher at space systems research and development department. His research interests are focused on satellite attitude determination and control, star tracker development, and satellite orbit estimation. He can be contacted at email: thquan@vnsc.org.vn.






Soat Le The    received engineer degree in automatic control from Hanoi University of Science and Technology (HUST) in 2011, and master's degree in space technology at Keio University in 2016. His interests are attitude and orbit control system (AOCS), mainly the algorithms for satellite attitude control such as reinforcement learning (RL), adaptive control, model predict control (MPC), and image processing for satellite images. He can be contacted at email: ltsoat@vnsc.org.vn.






Khang Trinh Van    graduated with a degree in aerospace engineering from Hanoi University of Science and Technology in 2012. He received master's degree in mechatronics at Le Quy Don University in 2016. Since 2023, he has been working at the Department of Space Systems Design of the Vietnam National Space Center. His research interests are in the field of space systems design, structures, and propulsion systems. He can be contacted at email: tvkhang@vnsc.org.vn.



Tu Tran Anh    received M.Sc. degree in space: earth observation–astrophysics – satellite technologies from University of Science and Technology of Hanoi (USTH) in 2021. Since 2018, he has been working at Vietnam National Space Center as researcher at Department of Space System Design. His research interests are in the fields of satellite attitude and orbit control system (AOCS), GNSS technology, and GNSS-based device. He can be contacted at email: tatu@vnsc.org.vn.



Linh La Thuy    received a M.Sc. degree in space: earth observation–astrophysics – satellite technologies from University of Science and Technology of Hanoi (USTH) in 2023. Since 2021, she has been working at Vietnam National Space Center as researcher at Department of Space System Design. Her research focuses on satellite's attitude, space mechanics, and optical system. She can be contacted at email: ltlinh@vnsc.org.vn.